RSC Advances

PAPER

View Article Online
View Journal | View Issue

Cite this: *RSC Adv.*, 2025, **15**, 9027

PD-L1 blockade peptide-functionalized $NaGdF_4$ nanodots for efficient magnetic resonance imaging-guided immunotherapy for breast cancer†

Zhenzhen Hu,[a] Yunkai Bao,[b] Xiaodong Li,[a] Zhuheng Li,*[c] Peihong Teng,[a] Guifeng Liu*[a] and Zhenxin Wang *[b]

Received 16th December 2024
Accepted 9th March 2025

DOI: 10.1039/d4ra08800j

rsc.li/rsc-advances

Immune checkpoint blockade (ICB) inhibitors have shown great promise for the treatment of numerous types of cancers, including triple-negative breast cancer (TNBC), by interrupting immunosuppressive checkpoints. Herein, programmed cell death ligand 1 (PD-L1) blockade peptide-functionalized $NaGdF_4$ nanodots (designated as PDL1-$NaGdF_4$ NDs) were prepared for magnetic resonance imaging (MRI)-guided TNBC immunotherapy through covalent conjugation of the PD-L1 blockade peptide (sequence, CALNNCVRARTR) with tryptone-capped $NaGdF_4$ NDs (designated as Try-$NaGdF_4$ NDs). MDA-MB-231 tumor could be easily tracked using *in vivo* MRI with PDL1-$NaGdF_4$ ND enhancement because the as-prepared PDL1-$NaGdF_4$ NDs have a high longitudinal relaxivity (r_1) value (22.8 mM^{-1} S^{-1}) and accumulate in the tumor site through binding with programmed cell death ligand-1 (PD-L1)-overexpressed cells. A series of *in vitro*/*in vivo* results demonstrated that the PDL1-$NaGdF_4$ NDs could effectively suppress MDA-MB-231 tumor growth in mice (66% volume ratio) by inhibiting migration and proliferation of tumor cells. In addition, the results of pharmacokinetic study showed that the PDL1-$NaGdF_4$ NDs were excreted from the body through the kidneys. These results highlight the potential of PDL1-$NaGdF_4$ NDs as a biocompatible nanomedicine for TNBC diagnosis and immunotherapy.

1. Introduction

Cancer immunotherapy has attracted continued attention in basic and clinical research and has gradually become one of the mainstream strategies for the treatment of cancer.[1–5] Generally, immunotherapy to suppress tumor is achieved through activation of the body's T cell-mediated durable immune response to attack tumors. However, the clinical outcomes of immunotherapy are strongly restricted by immunosuppressive checkpoints, which play a critical role in cancer immune suppression. Typically, the interaction between programmed death ligand 1 (PD-L1) overexpressed on tumor cells and programmed cell death protein-1 (PD-1) overexpressed on T cells can lead to the apoptosis of T cells and immune evasion of tumor cells.[1,4,6–11] Therefore, immune checkpoint blockade (ICB) inhibitors can trigger a durable antitumor response by interrupting immunosuppressive checkpoints. To date, several ICBs, including anti-PD-1 monoclonal antibodies and anti-PD-L1 monoclonal antibodies, have been approved for the treatment of various cancers as they block the PD-1/PD-L1 axis.[12,13] Although antibody-based ICB therapy has shown positive results in the treatment of multiple malignant cancers, it is restricted by the inherent drawbacks of the current therapeutic antibodies, such as their high cost, low stability, poor tumor permeability and the risk of immunogenicity.[14–20] Recently, peptide ICB inhibitors have been developed because of their easy production, low immune-related side effects and good tumor permeability.[14–17] For example, the peptides CLQKTPKQC and CVRARTR can reinvigorate T-cell activity and inhibit tumor progression by binding to PD-L1 with high affinity.[17]

As an aggressive subtype of breast cancers, triple-negative breast cancer (TNBC) accounts for 15–20% of all breast cancer types and has a worse prognosis than other subtypes of breast cancers.[21] Currently, there are only a small number of effective treatments against TNBC (*i.e.*, surgery and chemotherapy) because it lacks critical molecules that can be used for direct treatment, including the estrogen receptor (ER), progesterone receptor (PR), and human epidermal growth factor receptor 2 (HER2). Compared with other subtypes of breast cancers, TNBC has higher levels of PD-L1 expression.[21–25] This phenomenon suggests that TNBC patients might benefit from the inhibition of PD-1 binding to PD-L1.[21–29] Recently, several preclinical studies and clinical trials have shown that PD-1/PD-L1 ICB

[a]*Department of Radiology, China-Japan Union Hospital of Jilin University, Changchun 130033, P. R. China. E-mail: gfliu@jlu.edu.cn*

[b]*State Key Laboratory of Electroanalytical Chemistry, Changchun Institute of Applied Chemistry, Chinese Academy of Sciences, Changchun 130022, P. R. China. E-mail: wangzx@ciac.ac.cn*

[c]*Jilin Provincial Institute of Education, Changchun 130024, P. R. China. E-mail: lizhuheng@126.com*

† Electronic supplementary information (ESI) available. See DOI: https://doi.org/10.1039/d4ra08800j

inhibitor-based immunotherapy significantly prolongs the progression-free survival median of TNBC patients compared with those receiving standard chemotherapy.[24,28–30] Therefore, anti-PD-1/anti-PD-L1 is considered a promising therapeutic target for TNBC.

Magnetic resonance imaging (MRI) has been demonstrated as a powerful non-invasive diagnosis tool and has been extensively employed to diagnose various diseases, including cancers. In particular, the diagnosis sensitivity of MRI can be further improved using magnetic resonance contrast agents during the MRI process.[31–37] For example, Gd chelates can significantly enhance the T1-weighted MR signal because trivalent gadolinium ions (Gd^{3+}) have seven unpaired electrons with a large magnetic moment.[33–40] Although Gd chelates have achieved great success in the clinical field and commercial fields during the past few decades, they have several drawbacks, including low tumor accumulation capability, potential nephrotoxicity and a narrow imaging window.[33,41,42] Massive preclinical results have demonstrated that the drawbacks of Gd chelates can be overcome by the development of Gd^{3+}-containing nanomedicines.[33,35–40] In particular, Gd^{3+}-containing nanomaterials with a small size (<10 nm in diameter, also known as Gd nanodots (Gd NDs)) have been considered valuable substitutes to Gd chelates because Gd NDs can not only passively target tumor sites through their enhanced permeability and retention (EPR) effect, but can also be totally excreted from the body within a relatively short period (several hours to several days) through the renal clearance pathway.[43–49] In addition, Gd NDs can be further functionalized for achieving positive tumor-targeting ability and/or tumor treatment capability through suitable surface modification.

In this study, PD-L1 blockade peptide (sequence, CALNNCVRARTR)-functionalized $NaGdF_4$ NDs (termed as PDL1-$NaGdF_4$ NDs) were prepared for the MRI-guided immunotherapy of TNBC through conjugation of the PD-L1 blockade peptide on 5 nm tryptone-capped $NaGdF_4$ NDs (designated as Try-$NaGdF_4$ NDs) *via* covalent bonding. The PDL1-$NaGdF_4$ NDs exhibited unique features, including a high renal-clearance property, good biocompatibility, and strong T1-weighted MRI enhancement ability. *In vitro* and *in vivo* experimental results obtained using MDA-MB-231 tumor-bearing mice demonstrated that the PDL1-$NaGdF_4$ NDs could suppress TNBC tumor growth while inducing few unwanted side effects.

2. Experimental section

2.1 Reagents and materials

The PD-L1 blockade peptide (sequence CALNNCVRARTR, named anti-PD-L1, 90% purity) containing a linker peptide fragment (CALNN) and a PD-L1 antagonistic motif (CVRARTR) was purchased from Shanghai Qiangyao Biology (Shanghai, China). The MDA-MB-231 cell line was purchased from Shanghai Cell Bank, CAS (Shanghai, China). Details of other reagents used are provided in the ESI.† All reagents were of analytical grade, unless indicated otherwise, and were used without further purification. The details of the instruments used are also provided in the ESI.†

2.2 Synthesis of PDL1-$NaGdF_4$ NDs

Oleic acid (OA)-capped $NaGdF_4$ NDs (termed as OA-$NaGdF_4$ NDs) were synthesized by a previously reported solvothermal method (see ESI† for details).[44,45] The Try-$NaGdF_4$ NDs were prepared *via* OA-$NaGdF_4$ NDs using tryptone as a phase-transfer agent (see ESI† for details).[47–49] For synthesizing the PDL1-$NaGdF_4$ NDs, hydroxy-2,5-dioxopyrrolidine-3-sulfonicacid (sulfo-NHS, 6 mg mL^{-1}) and 1-(3-dimethylaminopropyl)-3-ethylcarbodiimide (EDC, 4 mg mL^{-1}) were freshly prepared using MES buffer (10 mM, pH 5.9). The 5 mL Try-$NaGdF_4$ NDs solution (1 mg mL^{-1}) was mixed with 2.5 mL sulfo-NHS solution and 2.5 mL EDC solution under vigorous stirring at 25 °C for 1.5 h. Then, 2.5 mL anti-PD-L1 solution (1 mg mL^{-1} in H_2O) was added into the mixture, and then vigorously stirred at 25 °C for another 12 h. Subsequently, the mixture was treated by centrifugation (10 000 rpm, 10 min). After discharging the supernatant, the as-obtained PDL1-$NaGdF_4$ NDs were washed 3 times by 5 mL PBS (10 mM PB containing 137 mM NaCl, pH 7.4) under centrifugation (10 000 rpm, 10 min), and redispersed into 5 mL PBS for the subsequent experiments. The as-prepared OA-$NaGdF_4$ NDs, Try-$NaGdF_4$ NDs and PDL1-$NaGdF_4$ NDs were fully characterized as described in the ESI.†

2.3 *In vitro* studies

For the wound-healing assay, MDA-MB-231 cells (8×10^4 cells per well) were seeded in to 6-well plates, and cultured with 5 mL RPMI 1640 culture medium supplemented with 10% (wt/v) FBS and 100 U per mL chlorostreptomycin for 24 h, respectively. After the cells reached confluence, a wound was generated in the cell layer by a 200 μL pipette tip, respectively. After washing the floating cells by 3 mL PBS (three times), the cells were continuously cultured in 5 mL RPMI 1640 culture medium supplemented with 100 U per mL chlorostreptomycin with Try-$NaGdF_4$ NDs and PDL1-$NaGdF_4$ NDs (100 ng mL^{-1}), respectively. Cells cultured in the blank culture medium were used as the control group. After incubation for 24 h, the cells were washed with 3 mL PBS, stained with 1 mL DAPI (5 μg mL^{-1}), and then imaged using a Nikon Ti–S fluorescence microscope. The cytotoxicities of the NDs were evaluated by a conventional MTT assay, and 1×10^6 NDs-stained MDA-MB-231 cells were carefully dispersed in 1% agarose hydrogel for *in vitro* MRI (see the ESI† for details). For the *in vitro* studies, the cell numbers were counted using a Cellometer Mini cell counter (Nexcelom).

2.4 *In vivo* measurements

BALB/c nude mice with an average bodyweight of 20 g were used to establish the MDA-MB-231 tumor model by subcutaneously inoculating 5×10^6 MDA-MB-231 cells suspended in PBS (100 μL) into the right flanks of the mice. All animal procedures were performed in accordance with the "Guidelines for Care and Use of Laboratory Animals" of the Changchun Institute of Applied Chemistry and approved by the Regional Ethics Committee for Animal Experiments of the Changchun Institute of Applied Chemistry (Ref. No. 20240007).

For *in vivo* tumor accumulation study, MDA-MB-231 tumor-bearing BALB/c nude mice were anesthetized using chloral hydrate (10 wt%), pre-injected intravenously with desired amounts (10 mg [Gd] per kg body weight) of PDL1-$NaGdF_4$ NDs and Try-$NaGdF_4$ NDs in PBS (100 μL) through the tail vein, and T1-weighted MR images were acquired at desired time points after injection using a Siemens 1.5 T MRI scanner (see ESI† for details).

For biotherapy study, the BALB/c nude mice with MDA-MB-231 tumor sizes of 3–4 mm in diameter were divided into three randomized groups: PBS, Try-$NaGdF_4$ NDs and PDL1-$NaGdF_4$ NDs, respectively. The tumor growth curves and Kaplan–Meier survival curves of the MDA-MB-231 tumor-bearing BALB/c nude mice were recorded (see ESI† for details).

3. Results and discussion

3.1 Synthesis and characterization of the PDL1-$NaGdF_4$ NDs

The PDL1-$NaGdF_4$ NDs were prepared according to previously reported methods with slight modifications.[48–50] Briefly, the hydrophilic Try-$NaGdF_4$ NDs were first prepared through a ligand exchange of hydrophobic OA molecules on the surface of the OA-$NaGdF_4$ NDs with hydrophilic casein phosphopeptides (CPPs)-containing phosphorylated serine residues (*e.g.*, –Ser(P)–Ser(P)–Ser(P)–Glu–Glu– fragment) in tryptone *via* the formation of robust Gd^{3+}–phosphate coordination bonds.[47] After activating the carboxyl groups of tryptone on the Try-$NaGdF_4$ NDs by EDC and sulfo-NHS, the PDL1-$NaGdF_4$ NDs were prepared by the formation of an amidation bond between the activated carboxyl group of the Try-$NaGdF_4$ NDs and the amine group at the N-terminal of anti-PD-L1.

As shown in Fig. 1, the as-prepared OA-$NaGdF_4$ NDs were spherical with an average size of 5 ± 0.5 nm in diameter and exhibited good monodispersibility. The XRD patterns of the NDs showed negligible changes after ligand exchange and anti-PD-L1 modification (as shown in Fig. S1†). These results indicate that the morphology of the $NaGdF_4$ NDs was not affected by ligand exchange and anti-PD-L1 modification. The average hydrodynamic diameters of the Try-$NaGdF_4$ NDs and PDL1-$NaGdF_4$ NDs were 6.2 ± 0.04 nm and 9.2 ± 0.04 nm, respectively. In addition, the polydispersity index (PDI) values of the Try-$NaGdF_4$ NDs and PDL1-$NaGdF_4$ NDs were 0.06 and 0.07, respectively. These results indicate that the NDs exhibited good monodispersity. Owing to the negatively charged nature of the phosphopeptide outer layer, the Try-$NaGdF_4$ NDs exhibited a negative zeta potential (as shown in Fig. S2†). The PDL1-$NaGdF_4$ NDs exhibited a positive zeta potential because of the positively charged nature of the anti-PD-L1 (PI = 10.9) outer layer (as shown in Fig. S2†). In addition, the MR signals of the NDs increased with increasing the concentration of NDs (as shown in Fig. 2). The longitudinal relaxivity (r_1) value of the PDL1-$NaGdF_4$ NDs (22.8 mM^{-1} S^{-1}) was much higher than that of the Try-$NaGdF_4$ NDs (10.8 mM^{-1} S^{-1}), indicating that the PDL1-$NaGdF_4$ NDs had excellent T1-weighted MRI enhancement ability. The difference in the r_1 values may be caused by the fact that the interaction of anti-PD-L1 with H_2O is stronger than that of tryptone with H_2O. These results are consistent with previously reported results.[48–50]

3.2 *In vitro* studies

As shown in Fig. 3, the proliferation of MDA-MB-231 cells decreased with increasing the concentration of PDL1-$NaGdF_4$ NDs, while there was a negligible change in the proliferation of MDA-MB-231 cells when increasing the concentration of Try-$NaGdF_4$ NDs. The MDA-MB-231 cells exhibited less than a 50% proliferation rate and 55% viability after incubation with 500 ng mL^{-1} (Gd content) PDL1-$NaGdF_4$ NDs for 24 h. These results suggest that the PDL1-$NaGdF_4$ NDs exhibited strong cytotoxicity towards MDA-MB-231 cells, and could efficiently inhibit the proliferation of MDA-MB-231 cells. Compared with the Try-$NaGdF_4$ NDs-stained MDA-MB-231 cells, the PDL1-$NaGdF_4$ NDs-

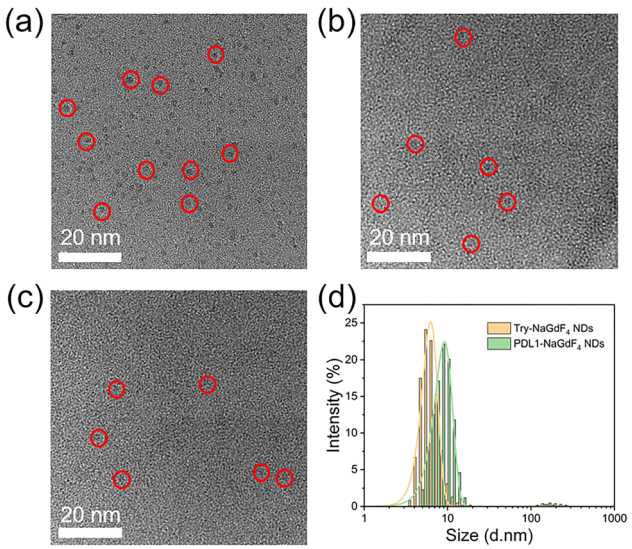

Fig. 1 TEM micrographs of the as-prepared (a) OA-$NaGdF_4$ NDs, (b) Try-$NaGdF_4$ NDs and (c) PDL1-$NaGdF_4$ NDs, and (d) hydrodynamic diameter distribution of Try-$NaGdF_4$ NDs and PDL1-$NaGdF_4$ NDs.

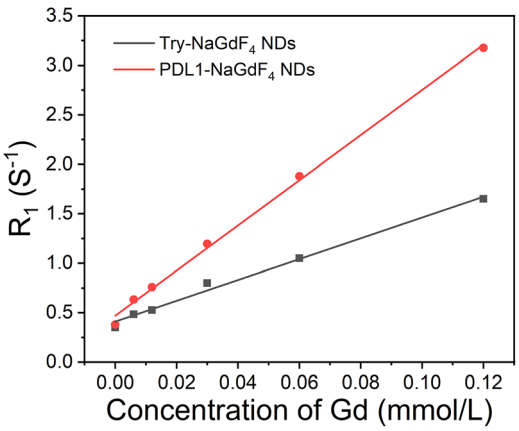

Fig. 2 R_1 relaxivities of Try-$NaGdF_4$ NDs (black line, r_1 = 10.8 mM^{-1} S^{-1}) and PDL1-$NaGdF_4$ NDs (red line, r_1 = 22.8 mM^{-1} S^{-1}) as a function of the molar concentration of Gd in the solution.

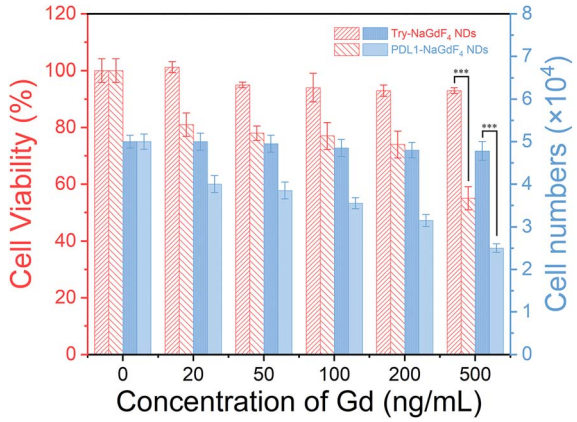

Fig. 3 Viability (red) and proliferation (blue) of MDA-MB-231 cells after incubation with various concentrations of Try-$NaGdF_4$ NDs and PDL1-$NaGdF_4$ NDs for 24 h, respectively (***$p < 0.001$). The concentrations of Try-$NaGdF_4$ NDs and PDL1-$NaGdF_4$ NDs are defined by their Gd content.

stained MDA-MB-231 cells exhibited a strong T1-weighted MR signal under the same experimental conditions (as shown in Fig. S3†), indicating the strong interactions of the PDL1-$NaGdF_4$ NDs with the MDA-MB-231 cells.

As shown in Fig. 4, a wound-healing assay was performed to evaluate the effect of the PDL1-$NaGdF_4$ NDs on the invasive capacity of MDA-MB-231 cells because TNBC normally exhibits strong invasiveness and metastasis. A wound was firstly generated in the cell layer using a pipette tip. The cells were then incubated with Try-$NaGdF_4$ NDs and PDL1-$NaGdF_4$ NDs, respectively. After 24 h culturing, the gap of the cells incubated with PDL1-$NaGdF_4$ NDs was found to be wider than those of cells incubated with Try-$NaGdF_4$ NDs and cells cultured in the blank culture medium. These results suggest that MDA-MB-231 cell migration was efficiently inhibited by the PDL1-$NaGdF_4$ NDs.

3.3 *In vivo* tumor-targeting capability and biodistribution of the PDL1-$NaGdF_4$ NDs

For evaluating their tumor-targeting capacity, the PDL1-$NaGdF_4$ NDs and Try-$NaGdF_4$ NDs were injected into MDA-MB-231 tumor-bearing BALB/c nude mice through the tail vein. *In vivo* T1-weighted MR images of the mice were recorded at specific time intervals within 24 h post-injection. As shown in Fig. 5, an enhancement in the T1-weighted MR signals at the tumor site could be clearly observed at 1 h post-injection of the NDs. The maximum enhancement of the T1-weighted MR signal was obtained at 2 h post-injection of the NDs and then gradually decreased to baseline within 24 h post-injection. In particular, the enhancement of the T1-weighted MR signal from the tumor sites of the PDL1-$NaGdF_4$ ND-treated mice was stronger than that of the Try-$NaGdF_4$ ND-treated mice during the period of 12 h post-injection. These results suggests that the PDL1-$NaGdF_4$ NDs could efficiently target PD-L1 overexpression in tumors (*e.g.*, TNBC), thus exhibiting good tumor-targeting capacity, and could be used as an excellent T1-weighted MRI

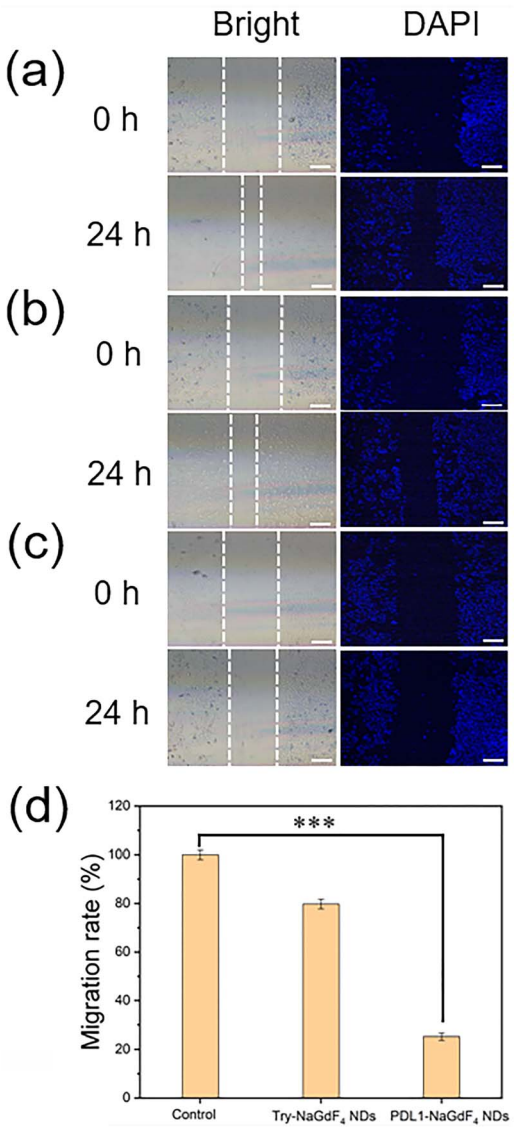

Fig. 4 Wound-healing assay of MDA-MB-231 cells treated with 100 ng per mL Try-$NaGdF_4$ NDs and PDL1-$NaGdF_4$ NDs for 24 h. MDA-MB-231 cells cultured in a blank culture medium were used as the control group. The bright-field and fluorescence images of the cells' gaps of the (a) control, (b) Try-$NaGdF_4$ NDs and (c) PDL1-$NaGdF_4$ NDs were taken at 0 and 24 h. The scale bar is 100 μm. (d) Corresponding quantification of the migration rate of MDA-MB-231 cells (***$p < 0.001$, $n = 3$).

contrast agent with a wide imaging window (at least 8 h). After the ND treatment, the enhancement in the T1-weighted MR signals in the kidneys of the mice was much stronger than those in the livers of the mice (as shown in Fig. S4 and S5†). These results suggest that both the Try-$NaGdF_4$ NDs and PDL1-$NaGdF_4$ NDs were excreted from body through the renal clearance pathway. Next, the Try-$NaGdF_4$ NDs- and PDL1-$NaGdF_4$ NDs-treated tumor-bearing mice were sacrificed at 2 h and 24 h post-injection, and their main organs and tumors were collected for analyzing the amount of Gd element by ICP-MS, respectively (as shown in Fig. S6†). The amount of Gd in the tumors of the PDL1-$NaGdF_4$ NDs-treated mice was higher than

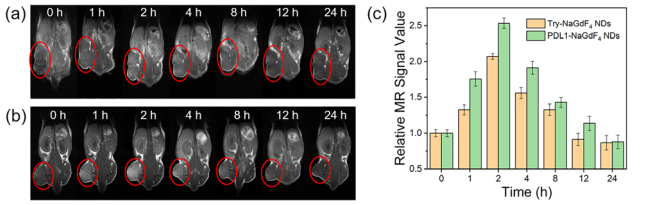

Fig. 5 *In vivo* MR images of MDA-MB-231 tumor-bearing BALB/c mice after the intravenous injection of (a) Try-$NaGdF_4$ NDs and (b) PDL1-$NaGdF_4$ NDs (10 mg [Gd] per kg body weight) at 0 (preinjection), 1, 2, 4, 8, 12 and 24 h post-injection, and (c) corresponding data analysis of the relative MR signals of the tumors. The MR signal at 0 h (preinjection) is defined as 1.

that in the Try-$NaGdF_4$ NDs-treated mice, confirming the high tumor-targeting capability of the PDL1-$NaGdF_4$ NDs. The amount of Gd in the kidneys was higher than that in the livers. These results also indicated the renal clearance of the NDs. In addition, the amount of Gd in the kidneys of the Try-$NaGdF_4$ NDs-treated mice was higher than that in the PDL1-$NaGdF_4$ NDs-treated mice, indicating that the clearance rate of Try-$NaGdF_4$ NDs was faster than that of the PDL1-$NaGdF_4$ NDs. This phenomenon was consistent with the experimental results from the *in vivo* MRI.

3.4 Biotherapy of the PDL1-$NaGdF_4$ NDs

The pharmacokinetics of the PDL1-$NaGdF_4$ NDs was first investigated before using the PDL1-$NaGdF_4$ NDs for tumor treatment. In this case, the Try-$NaGdF_4$ NDs and PDL1-$NaGdF_4$ NDs were injected into healthy nude mice through the tail vein. Urine and blood samples were collected for analyzing the amounts of Gd at different time points within 24 h post-injection. As shown in Fig. 6, the amount of Gd in the blood gradually decreased over time, while the amount of Gd in the urine increased over time. The amounts of Gd in the blood decreased to below 5% of the injection dose (ID) at 8 h post-injection. However, throughout the entire testing period, the amount of Gd in the blood of the PDL1-$NaGdF_4$ NDs-treated mice was slightly higher than that of the Try-$NaGdF_4$ NDs-treated mice, indicating that the PDL1-$NaGdF_4$ NDs had a longer blood circulation time than the Try-$NaGdF_4$ NDs. Also, 84.2% ID of the Try-$NaGdF_4$ NDs and 81.7% of the PDL1-$NaGdF_4$ NDs were found in the urine at 24 h post-injection. These results confirmed that both the Try-$NaGdF_4$ NDs and PDL1-$NaGdF_4$ NDs could be excreted from the body through the renal clearance pathway. The efficient renal clearance of PDL1-$NaGdF_4$ NDs eliminates the potential long-term *in vivo* toxicity of the PDL1-$NaGdF_4$ NDs. In addition, healthy BALB/c mice were treated with a single dose of Try-$NaGdF_4$ NDs and PDL1-$NaGdF_4$ NDs, and then sacrificed for histology analysis at 30-day post-injection. There were negligible histological changes found on the main organs of the mice at 30-day post-injection of the PDL1-$NaGdF_4$ NDs, also indicating the low *in vivo* toxicity of the PDL1-$NaGdF_4$ NDs (as shown in Fig. S7†).

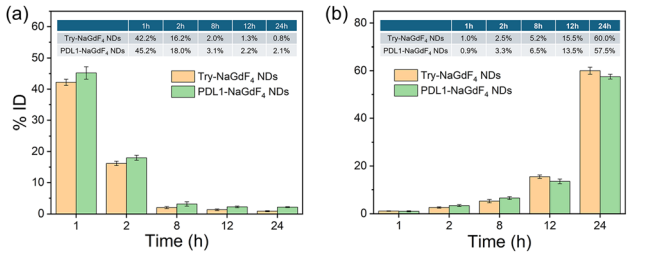

Fig. 6 ICP-MS measurements of the amount of Gd in the (a) blood samples and (b) urine samples of healthy BALB/c mice within 24 h intravenous injection of Try-$NaGdF_4$ NDs and PDL1-$NaGdF_4$ NDs (10 mg [Gd] per kg body weight).

In summary, MDA-MB-231 tumor-bearing mice were randomly divided into three groups: PBS only, Try-$NaGdF_4$ NDs and PDL1-$NaGdF_4$ NDs treatment, respectively. Compared with the PBS- and Try-$NaGdF_4$ NDs-treatment groups, the growth of MDA-MB-231 tumors were inhibited significantly after treatment with the PDL1-$NaGdF_4$ NDs (as shown in Fig. 7). It was found that the PDL1-$NaGdF_4$ NDs could effectively suppress MDA-MB-231 tumor growth in the mice with an inhibition rate of 66% (volume ratio) after 15 days of treatment. Even though the physical presence of the PDL1-$NaGdF_4$ NDs in the body was temporary, their inhibitory effect on PD-L1 activated the immune system and enhanced T cell function. The activated T cells enable the continuous recognition and elimination of tumor cells, thereby exerting a long-term suppression of tumor growth. The tumor slices under different treatments were tested by TUNEL staining. As shown in Fig. 8, a few apoptotic cells were observed in the PBS- and Try $NaGdF_4$ NDs-treatment

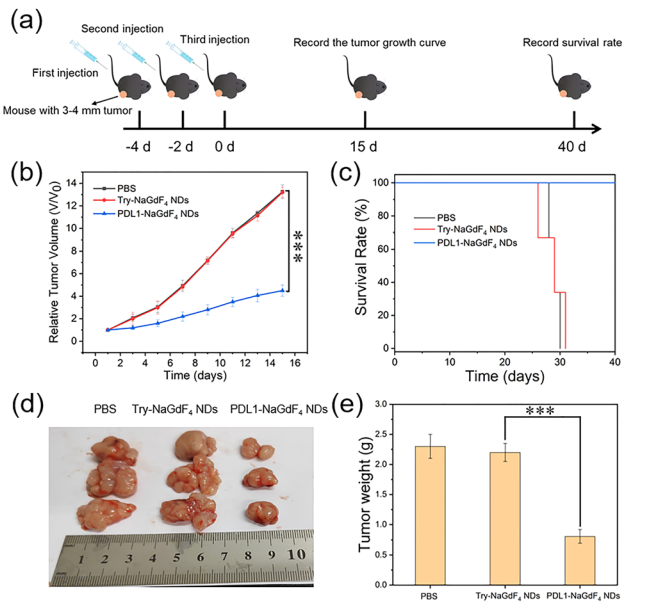

Fig. 7 (a) Schematic representation of the MDA-MB-231 tumor-bearing mice breast cancer treatment. (b) Tumor growth curves and (c) survival curves of the mice under different treatments, and (d) digital photographs and (e) weights of the tumors after 15 days of treatment. The MDA-MB-231 tumor-bearing mice were treated with PBS, Try-$NaGdF_4$ NDs and PDL1-$NaGdF_4$ NDs. The injection dose of NDs was 10 mg [Gd] per kg body weight (***$p < 0.001$).

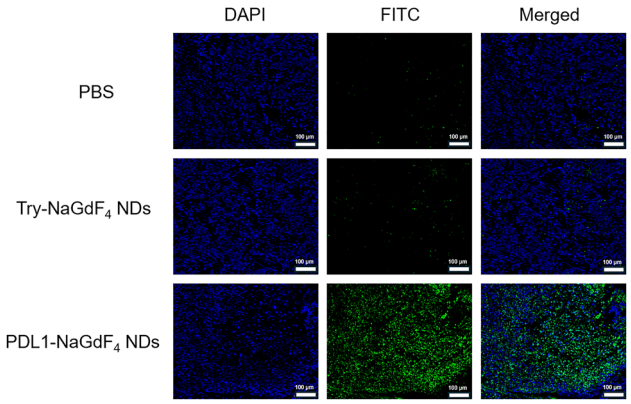

Fig. 8 TUNEL staining images of tumor slices after 15 days of treatment. MDA-MB-231 tumor-bearing mice were treated with PBS, Try-$NaGdF_4$ NDs and PDL1-$NaGdF_4$ NDs. The injection dose of NDs was 10 mg [Gd] per kg body weight.

groups, while massive apoptotic cells were observed in the PDL1-$NaGdF_4$ NDs-treatment group. In particular, the 40-day survival rate of the PDL1-$NaGdF_4$ NDs-treated tumor-bearing mice (100%) was higher than those of the PBS-treated mice (0%) and Try $NaGdF_4$ NDs-treated mice (0%). The results indicate that the PDL1-$NaGdF_4$ NDs have good therapeutic effects, and can inhibit tumor growth, and prolong the survival time of MDA-MB-231 tumor-bearing mice.

4. Conclusions

In summary, we developed nanoscale diagnostic and therapeutic agents called PDL1-$NaGdF_4$ NDs, which were capable of achieving MRI-guided ICB therapy through covalent conjugation of the PD-L1 blockade peptide anti-PD-L1 with Try-$NaGdF_4$ NDs. *In vitro* experimental results showed that the PDL1-$NaGdF_4$ NDs exhibited high MRI enhancing capacity and could significantly inhibit the migration and proliferation of MDA-MB-231 cells. *In vivo* experimental results demonstrated that the PDL1-$NaGdF_4$ NDs could effectively enhance the MR signal of MDA-MB-231 tumor-bearing mice and clearly could suppress tumor growth. Furthermore, the PDL1-$NaGdF_4$ NDs could be efficiently excreted from the body through the renal clearance pathway, which eliminates the potential long-term *in vivo* toxicity of the PDL1-$NaGdF_4$ NDs. Overall, this study provides a promising strategy for the design of nanomedicines to better combat PD-L1-overexpression TNBC. Further exploration and validation through more complex TNBC models (*e.g.*, remote metastatic tumor) will be needed to fully elucidate the clinical implications of the PDL1-$NaGdF_4$ NDs in the field of breast cancer treatment.

Data availability

The datasets used during the current study are available from the corresponding author upon reasonable request. The ESI† is available free of charge in the online vision.

Author contributions

Zhenzhen Hu: theoretical calculations, experimental verification, manuscript writing, and proofreading. Yunkai Bao: data management, review and editing. Xiaodong Li: theoretical calculations and data management. Zhuheng Li: supervision, project management and fund acquisition. Peihong Teng: investigating, reviewing and editing. Guifeng Liu and Zhenxin Wang: project management, fund acquisition, supervision, reviewing and editing.

Conflicts of interest

There are no conflicts to declare.

Acknowledgements

The authors would like to thank the Science and Technology Developing Foundation of Jilin Province (Grant No. 20220101078JC) for financial support.

Notes and references

1 D. M. Pardoll, *Nat. Rev. Cancer*, 2012, **12**, 252–264.
2 A. Mantovani, P. Allavena, F. Marchesi and C. Garlanda, *Nat. Rev. Drug Discovery*, 2022, **21**, 799–820.
3 Y. Li, H. J. Zhang, Y. Merkher, L. Chen, N. Liu, S. Leonov and Y. H. Chen, *J. Hematol. Oncol.*, 2022, **15**, 121.
4 P. Sharma, S. Goswami, D. Raychaudhuri, B. A. Siddiqui, P. Singh, A. Nagarajan, J. L. Liu, S. K. Subudhi, C. Poon, K. L. Gant, S. M. Herbrich, S. Anandhan, S. Islam, M. Amit, G. Anandappa and J. P. Allison, *Cell*, 2023, **8**, 1652–1669.
5 A. Fenis, O. Demaria, L. Gauthier, E. Vivier and E. Narni-Mancinelli, *Nat. Rev. Immunol.*, 2024, **24**, 471–486.
6 M. A. Postow, R. Sidlow and M. D. Hellmann, *N. Engl. J. Med.*, 2018, **378**, 158–168.
7 P. Sharma and J. P. Allison, *Science*, 2015, **348**, 56–61.
8 A. Ribas and J. D. Wolchok, *Science*, 2018, **359**, 1350–1355.
9 A. C. Huang and R. Zappasodi, *Nat. Immunol.*, 2022, **23**, 660–670.
10 Q. Sun, Z. Y. Hong, C. Zhang, L. L. Wang, Z. Q. Han and D. Ma, *Signal Transduction Targeted Ther.*, 2023, **8**, 320.
11 A. Zhang, T. Fan, Y. X. Liu, G. H. Yu, C. X. Li and Z. Jiang, *Mol. Cancer*, 2024, **23**, 251.
12 K. M. Hargadon, C. E. Johnson and C. J. Williams, *Int. Immunopharmacol.*, 2018, **62**, 29–39.
13 J. Y. Qiu, Z. L. Cheng, Z. Jiang, L. H. Gan, Z. X. Zhang and Z. Z. Xie, *Int. J. Mol. Sci.*, 2024, **25**, 5490.
14 X. K. Zhang, Y. Wu, J. Y. Lin, S. X. Lu, X. C. Lu, A. Y. Cheng, H. Z. Chen, W. D. Zhang and X. Luan, *Acta Pharm. Sin. B*, 2024, **14**, 3818–3833.
15 J. Fetse, Z. Zhao, H. Liu, U. Mamani, B. Mustafa, P. Adhikary, M. Ibrahim, Y. L. Liu, P. Patel, M. Nakhjiri, M. Alahmari, G. F. Li and K. Cheng, *J. Med. Chem.*, 2022, **65**, 12002–12013.
16 Z. Hu, W. Q. Li, S. M. Chen, D. H. Chen, R. Xu, D. L. Zheng, X. Yang, S. Z. Li, X. M. Zhou, X. S. Niu, Y. M. Xiao, Z. Y. He,

H. H. Li, J. Liu, X. H. Sui and Y. F. Gao, *Sci. China:Life Sci.*, 2023, **66**, 2310–2328.
17 S. Gurung, F. Khan, G. R. Gunassekaran, J. D. Yoo, S. M. P. Vadevoo, U. Permpoon, S. H. Kim, H. J. Kim, I. S. Kim, H. Han, J. H. Park, S. Kim and B. Lee, *Biomaterials*, 2020, **247**, 119984.
18 J. Yang and L. Q. Hu, *Med. Res. Rev.*, 2019, **39**, 265–301.
19 Y. Z. Wu, Y. Zhang, Y. Guo, Z. C. Pan, S. C. Zhong, X. X. Jin, W. H. Zhuang, S. K. Chen, J. Gao, W. H. Huang, X. W. Dong and J. X. Che, *Eur. J. Med. Chem.*, 2021, **223**, 113637.
20 S. Javed, A. Najmi, W. Ahsan and K. Zoghebi, *Front. Immunol.*, 2024, 1383456.
21 S. Dees, R. Ganesan, S. Singh and I. Grewal, *Thorac. Cancer*, 2021, **7**, 162173.
22 L. A. Emens, *Clin. Cancer Res.*, 2018, **24**, 511–520.
23 M. Nakhjavani and S. Shigdar, *Pharmacol. Res.*, 2022, **175**, 106019.
24 V. C. Rayson, M. A. Harris, P. Savas, M. L. Hun, B. Virassamy, R. Salgado and S. Loi, *Thorac. Cancer*, 2024, **10**, 490–506.
25 P. Schmid, S. Adams, H. S. Rugo, A. Schneeweiss, C. H. Barrios, H. Iwata, V. Diéras, R. Hegg, S. Im, G. S. Wright, V. Henschel, L. Molinero, S. Y. Chui, R. Funke, A. Husain, E. P. Winer, S. Loi and L. A. Emens, *N. Engl. J. Med.*, 2018, **22**, 2108–2121.
26 Y. N. Sun, B. C. Lyu, C. Yang, B. He, H. Zhang, X. Q. Wang, Q. Zhang and W. B. Dai, *Bioact. Mater.*, 2023, **22**, 47–59.
27 Z. W. Qiu, Z. M. Lu, J. Q. Huang, Y. T. Zhong, N. Yan, R. J. Kong and H. Cheng, *Biomaterials*, 2023, **303**, 122392.
28 A. Okines and N. Turner, *Lancet Oncol.*, 2024, **25**, 149–151.
29 S. L. Zhu, Y. Z. Wu, B. Song, M. Yi, Y. H. Yan, Q. Mei and K. M. Wu, *J. Hematol. Oncol.*, 2023, **16**, 100.
30 S. Kumar, M. Chatterjee, P. Ghosh, K. K. Ganguly, M. Basu and M. K. Ghosh, *Genes Dis.*, 2023, **10**, 1318–1350.
31 Q. Dan, X. P. Jiang, R. Wang, Z. F. Dai and D. S. Su, *Adv. Sci.*, 2023, **10**, 2207090.
32 C. Q. Zhang and K. Y. Cai, *Adv. Mater.*, 2023, **35**, 2205409.
33 X. D. Li, Y. H. Sun, L. N. Ma, G. F. Liu and Z. X. Wang, *Molecules*, 2020, **25**, 5072.
34 G. X. Si, Y. Du, P. Tang, G. Ma, Z. C. Jia, X. Y. Zhou, D. Mu, Y. Shen, Y. Lu, Y. Mao, C. Chen, Y. Li and N. Gu, *Natl. Sci. Rev.*, 2024, **11**, nwae057.
35 P. Caravan, *Chem. Soc. Rev.*, 2006, **35**, 512–523.
36 G. H. Lee, Y. M. Chang and T. J. Kim, *Eur. J. Inorg. Chem.*, 2012, 1924–1933.
37 Y. Cao, L. J. Xu, Y. Kuang, D. S. Xiong and R. J. Pei, *J. Mater. Chem. B*, 2017, **5**, 3431–3461.
38 P. Verwilst, S. Park, B. Yoon and J. S. Kim, *Chem. Soc. Rev.*, 2015, **44**, 1791–1806.
39 J. Y. Ding, Z. J He, Y. J. Zhai, L. Ye, J. B. Ji, X. Y. Yang and G. X. Zhai, *Coord. Chem. Rev.*, 2024, **501**, 215594.
40 X. Y. Li, Q. S. Liu, M. L. Wu, H. Wang, J. Yang, X. Y. Mu and X. D. Zhang, *Adv. Healthcare Mater.*, 2024, 2403099.
41 A. Fatima, M. W. Ahmad, A. K. A. Al Saidi, A. Choudhury, Y. Chang and G. H. Lee, *Nanomaterials*, 2021, **11**, 2449.
42 M. Rogosnitzky and S. Branch, *Biomaterials*, 2016, **29**, 365–376.
43 J. Y. Park, M. J. Baek, E. S. Choi, S. Woo, J. H. Kim, T. J. Kim, J. C. Jung, K. S. Chae, Y. M. Chang and G. H. Lee, *ACS Nano*, 2009, **3**, 3663–3669.
44 H. Xing, S. Zhang, W. Bu, X. Zheng, L. Wang, Q. Xiao, D. Ni, J. Zhang, L. Zhou, W. Peng, K. Zhao, Y. Hua and J. Shi, *Adv. Mater.*, 2014, **26**, 3867.
45 N. J. J. Johnson, W. Oakden, G. J. Stanisz, R. S. Prosser and F. C. J. M. van Veggel, *Chem. Mater.*, 2011, **23**, 3714–3722.
46 F. F. He, L. C. Zhu, X. H. Zhou, P. S. Zhang, J. W. Cheng, Y. Y. Qiao, Y. C. Feng, S. S. Yue, M. Xu, J. Q. Guan, X. M. Li, Z. Ao, M. Qin, Y. Hou and D. Han, *ACS Appl. Mater. Interfaces*, 2022, **14**, 26372–26381.
47 F. Y. Liu, X. X. He, J. P. Zhang, H. M. Zhang and Z. X. Wang, *Small*, 2015, **11**, 3676–3685.
48 H. D. Chen, X. D. Li, F. Y. Liu, H. M. Zhang and Z. X. Wang, *Mol. Pharm.*, 2017, **14**, 3134–3141.
49 Y. Fu, Xi. D. Li, H. D. Chen, Z. X. Wang, W. S. Yang and H. M. Zhang, *ACS Appl. Bio Mater.*, 2019, **2**, 3613–3621.
50 Xi. D. Li, Y. K. Bao, Z. H. Li, P. H. Teng, L. N. Ma, H. Zhang, G. F. Liu and Z. X. Wang, *Sci. Rep.*, 2024, **14**, 15764.